Supporting Information

Zanchetta et al. 10.1073/pnas.1011199107

SI Text

1 SI Results. ***1.1 Description of the sequences explored in this work.*** Sequences listed in Table 1 have been chosen so to test various properties of the sequences:

- Length
- Nature of the end-to-end coupling [blunt-ended (BE) vs. sticky-dangling (SD)]
- Self vs. mutual complementarity
- Sequence composition at the duplex terminals
- Sequence composition at the duplex center
- Effects of relative AT and CG content
- Effect of phosphorylation of the terminals

The sequence **5** (s**5**) in Table 1 is the OH-terminated "Drew–Dickerson" (DD) dodecamer, whose structure has been thoroughly studied at various levels of hydration and can be considered an archetypal example of the B-form DNA (1). Different variations of the DD sequence have been also studied: s**6** and s**7**, corresponding to DD phosphorylated at the 5′ (pDD) or at the 3′ (DDp) terminals, respectively; s**8**, corresponding to an antisymmetric inversion of the DD sequence; s**27**, the RNA counterpart of DD; s**10**–s**13** in which, by changing one nucleotide at a time, we gradually study the difference between DD and the sequence "allAT" containing only A and T; s**1**, s**2**, s**3**, s**17**, s**18**, s**19**, s**25**, obtained by shortening or elongating DD in various ways; s**16**, s**20**–s**23**, variants of DD so to produce SD end coupling. In particular, s**16** is obtained by a shift in the DD sequence ("shifted DD," sDD) so to match, when aggregated, the same base sequence of an aggregate of DD. In fact, for a 3-duplex aggregate of DD via end-to-end stacking we get

```
CGCGAATTCGC|GCGCGAATTCGCG|CGCGAATTCGCG
GCGCTTAAGCG|CGCGCTTAAGCGC|GCGCTTAAGCGC
```

where the red lines indicate the terminals of the oligomers. A 3-duplex aggregate of sDD through the pairing of the sticky ends would instead lead to

```
GCGCGAATTCGC|GCGCGAATTCGC|GCGCGAATTCGC
   CGCTTAAGCGCG|CGCTTAAGCGCG|CGCTTAAGCGCG
```

The two aggregates have the same nucleotide sequence and differ only in the position of the chemical discontinuities. Other sequences have been chosen to test structures markedly different from DD. Among them: s**9**, a mutually complementary pair of 12-mers (12 mc); the sequences s**14** and s**15**, containing only C and G nucleotides (allCG1 and allCG2); s**4**, a shortened variant of allAT; s**24** and s**26**, self-complementary 16-mer and 20-mer with no significant overlap with DD.

1.2 Conventions on handedness. Conventions on handedness are as follows: (*i*) Circular polarization. The polarization is left-handed (LH) if, for light propagating toward the observer, the electric field on a given plane rotates anticlockwise, as sketched in Fig. 1*B*. (*ii*) Handedness of the *N* phase. The *N* is LH if, upon moving perpendicularly to the director (i.e., along the helical axis) toward the observer, *n* rotates clockwise. Given these conventions, the LH *N* phase selectively reflects LH circularly polarized light.

1.3 Description of the propagation model. Following Yang and Mi (2), we have implemented the calculation of the transmitted and reflected spectra for light propagating through a cell of thickness d in the direction of the helical axis of a chiral nematic having pitch p and local nematic birefringence Δn. The calculation, is carried out by dividing the cell into thin layers, each described as a uniaxial retarder, and by computing the net propagation with the Jones matrix method in the limit of vanishingly thin layers. The comparison between the model predictions and the experimental spectra enables to extract pitch, local birefringence, and handedness.

The calculation of $I_T(\theta)$, the intensity of the transmitted field through crossed or decrossed polarizers, is carried out along the line described in (2). In this work, the authors consider a cholesteric liquid crystal cell of thickness d with helical axis along the z-axis of the Cartesian coordinates. They divide the cholesteric liquid crystal into N slabs of thickness $\Delta z = d/N$, modeling each slab as a nematic liquid crystal. They derive the following recursive formula

$$\begin{bmatrix} E_t(z) \\ E_r(z) \end{bmatrix} = M \begin{bmatrix} E_t(z+\Delta z) \\ E_r(z+\Delta z) \end{bmatrix} \qquad \textbf{[S1]}$$

where $E_t(z)$ and $E_r(z)$ are the Jones vectors associated, respectively, with the transmitted and reflected electric fields from the $z/\Delta z$th slab, with $M = \begin{bmatrix} A & B \\ B^* & A^* \end{bmatrix}$, A and B being 2×2 matrices defined in equations 18 and 19 of ref. 1, respectively.

In the original description the Jones vectors in each slab are referred to a local frame of reference with one axis oriented along the nematic director. We adopt here a fixed frame of reference and assume a fixed tilt angle $2\pi h/p$ between the nematic directors of neighboring slabs. In this case the matrix M can be written, up to first order in Δz, as $M = I + S\Delta z$, where I is the unit matrix and

$$S = 2\pi \begin{bmatrix} jn_e/\lambda & \Delta n/2n_e p & 0 & \Delta n/2n_e p \\ \Delta n/2n_o p & jn_o/\lambda & \Delta n/2n_o p & 0 \\ 0 & \Delta n/2n_e p & -jn_e/\lambda & \Delta n/2n_e p \\ \Delta n/2n_o p & 0 & \Delta n/2n_o p & -jn_o/\lambda \end{bmatrix}.$$

Here j is the imaginary unit. Composition of Eq. **S1** from $z = 0$ to $z = h$ leads to

$$\begin{bmatrix} E_t(0) \\ E_r(0) \end{bmatrix} = T \begin{bmatrix} E_t(h) \\ E_r(h) \end{bmatrix}$$

where $T = M^N \cong (I + Sd/N)^N$. In the continuous limit $N \to \infty$,

$$T \to \exp(Sh) \equiv \begin{bmatrix} T_1 & T_2 \\ T_3 & T_4 \end{bmatrix}.$$

In this limit T can be easily evaluated after numerical diagonalization of S. By imposing: $E_t(0) = E_i$, $E_r(0) = E_r$, $E_t(d) = E_t$, $E_r(d) = 0$ (E_i, E_r, E_t being respectively the incident, reflected and transmitted field), we obtain:

$$E_t = T_1^{-1} E_i \qquad E_r = T_3 T_1^{-1} E_i$$

This scheme allows calculating the reflected and the transmitted field for an arbitrary polarization state of incident field. In particular, if the incident field is linearly polarized along a given direction (say, the x-axis): $E_i = [1 \quad 0]^T$, and the transmitted intensity is measured after passing a polarizer tilted by an angle θ with respect to the y-axis, one gets

$$\tau(\theta) = |A(\theta)T_1^{-1}E_i|^2$$

where A_θ is the Jones matrix associated with the analyzing polarizer:

$$A(\theta) = \begin{bmatrix} \sin^2(\theta) & \sin(\theta)\cos(\theta) \\ \sin(\theta)\cos(\theta) & \cos^2(\theta) \end{bmatrix}.$$

1.4 Pitch in the μm range. When the pitch of the N^* phase is in the μm range, the measurement of spectra in the visible range is not as informative as for shorter pitch. The spectra are in this case quite featureless, but measurements of the intensity vs. ϑ are useful because they enable determining the optical rotation, in turn related to handedness, Δn, d, and p. This phenomenon can be recognized in Fig. 2*A* of the main article, by noticing that for $\lambda < \lambda_0$ and outside the selective reflection interval, the transmitted intensity is larger for $\vartheta > 0$. Opposite behavior is found in Fig. 2*B*.

Hence in the case of right-handed (RH) N^* helices, for λ below the reflection band, RH circularly polarized light propagates with a lower effective refractive index than LH polarized light, giving rise to a optical rotation in the direction opposite to that of the N^* helix (3). This condition is attained when the pitch is larger than the wavelength ($p > 2\lambda$) but at the same time not too large, namely when $p\Delta n \ll \lambda$. In this regime (matched by our samples), the rotatory power ρ, defined as the angle of rotation per unit length—where positive ρ means a LH rotation—is simply expressed as a function of the basic optical properties of the N^* structure.

In the case of N^* pitch longer than visible range (with $p > 2\lambda$ and $p\Delta n \ll \lambda$), the optical rotation is well approximated by (2):

$$\rho = -\frac{\pi(\Delta n)^2 p}{4\lambda^2}. \qquad \textbf{[S2]}$$

In Fig. S1 we report a comparison between the optical rotation computed with Eq. **S2** (red line) and through the model described above (blue line). The parameters used to perform the calculation with both models are $n = 1.5$, $\Delta n = 0.038$, $h = 15$ μm, $\lambda = 0.5$ μm.

We have measured the optical rotation of DNA N^* phase for all sequences that organize with a long pitch. In Fig. 1*E* of the main article we show a chiral nematic texture typically observed in DD cells when observed through crossed polarizers. In the uniform domain areas, surrounded by oily streak type defects, where fingerprint-like lines are visible, the N^* helix is normal to the surfaces. In this type of cell, a residual transmission is observed, appreciable when compared to the dark background of the isotropic phase. As the analyzer is rotated, the transmitted intensity changes, so that the position of minimum transmission ϑ_{MIN} is easily determined (Fig. 1*F*). Measurements performed here satisfy the condition $p\Delta n \ll \lambda$ that in the case of DNA becomes $p \gg 15$ μm. For DD and 10sc duplexes we find positive ϑ_{MIN} and hence negative ρ, indicating RH cholesteric phase. On the contrary, for longer strands as 14sc and 16sc, and for other dodecamer sequences, we find opposite handedness. As in the case of the compounds with shorter p, the procedure was validated by testing with LH and RH thermotropic mixtures.

The optical analysis introduced above has lead us to recognize a certain intrinsic variability in pitch length from cell to cell, probably depending on the boundary surface, cell thickness, preparation conditions and possibly in the purity of the samples. This variability is included in the range of p values in Table 1. Never, however, we observed contrasting handedness for a given sequence at given c and T.

1.5 Discussion of the expansion coefficients. The nano-DNA (nDNA) samples exhibiting a cholesteric phase with pitch in the visible range have the typical appearance of Fig. 1*A* of the main article. They are composed by different cholesteric patches with the helical axis normal to the confining cell walls separated by "oily streaks," sort of grain boundaries where the LC is organized into cholesteric stripes whose helical axis lies in a plane parallel to cell walls and is orthogonal to the stripe direction. The spectrum of the intensity of the transmitted light from such a composite sample is given by the sum of the contributions from these different regions, weighted with the respective surface fraction.

If the helix pitch is in the visible range (or shorter), from an optical point of view the oily streaks behave as birefringent wave plates, whose birefringence is given approximately by $\Delta n_{\mathrm{eff}} = \Delta n/2$, where Δn is the birefringence of a single nematic plane. The fast axis of each wave plate coincides with the streak direction.

The contribution to the spectrum of the transmitted light from a single birefringent domain is given by:

$$\tau_B(\theta|\alpha) = \frac{I(\theta)}{I_0} = \sin^2(\theta) + \frac{1}{2}\sin(2\alpha)\sin(2\alpha - \theta)[1 - \cos(\varphi)]. \qquad \textbf{[S3]}$$

Here α is the angle between fast axis and polarizer, $\varphi = 2\pi h\Delta n_{\mathrm{eff}}/\lambda$ is the phase retard, θ is the decrossing angle between polarizer and analyzer. For small θ Eq. **S3** can be expanded as:

$$\tau_B(\theta|\alpha) \cong \frac{1}{2}\sin^2(2\alpha)(1 - \cos\varphi) - \frac{1}{2}\sin(4\alpha)(1 - \cos\varphi)\theta + [1 - \sin^2(2\alpha)(1 - \cos\varphi)]\theta^2. \qquad \textbf{[S4]}$$

If the sample area of interest includes a large enough number of cholesteric patches, each of these being surrounded by a birefringent contour as typically observed in this work, than there is no preferential orientation in the birefringent streaks. As a consequence, when the global contribution of all these birefringent domains is considered, the term of the first order in θ in Eq. **S4**, which is proportional to $\sin(4\alpha)$, tends to average to zero. This means that the transmission spectrum between quasi-crossed polarizer does not depend on the direction of the analyzer rotation (either clockwise or counterclockwise) but only on the absolute value of the rotation angle.

This behavior is very different from that of a cholesteric domain, whose transmission spectrum $\tau_C(\theta)$ clearly shows a shift of the selective reflection band when the analyzer is rotated. This shift is approximately linear in the rotation angle θ and the sign of the proportionality constant is univocally attributed to the handedness of the cholesteric phase. The first order term in θ in the $\tau_C(\theta)$ expansion is thus highly informative, as it allows the direct determination of the sample handedness, among other relevant quantities (helix pitch and birefringence).

Based in this observation, the data analysis procedure described in the text relies on the fit of the first order term in θ of the measured $\tau(\theta)$. From each sample a number of spectra $\tau(\theta)$ are recorded for different rotation angles $\theta_1,\theta_2,\ldots,\theta_N$ (tipically $\theta_1,\theta_2,\ldots,\theta_N = -10°, -8°,\ldots,10°$) and the first odd term τ_1 in the θ expansion is numerically evaluated for each wavelength. According to the discussion above τ_1 is expected to incorporate the contribution from the cholesteric domains alone and can be thus directly compared with the analogous quantity calculated from a defect-free cholesteric sample as described in the previous paragraph.

Among the sequences in Table 1, pitches in the visible range are displayed by: 8sc2, 10sc, pDD, DDp, allAT, allCG2, DD-RNA, sDD, and GC-DD. For each of them, $I_T(\lambda,\vartheta)$ spectra have been measured for $-10° \le \vartheta \le +10°$ (2° increments) at room

temperature, in samples with concentration roughly at the center of the interval yielding the N^* phase.

1.6 Effect of the boundary conditions. The boundary conditions in nDNA LC cells cannot be controlled as in standard thermotropics. The resulting boundary conditions are of planar alignment with random orientation of DNA helices on the cell walls, leading to the breaking of the N^* phase into domains with different alignment directions. In particular, two main deviations from an ideal N^* helix are observed:

1. the formation of a network of birefringent defects enclosing uniformly aligned N^* domains;
2. a polydispersity of the pitch of different domains of the order of $\Delta p \sim p^2/d$.

The effect of both the defect network and the pitch strain on the spectrum of transmitted light can be appreciated in Fig. S2, showing the spectra from two different cells containing the same thermotropic mixture M2 (2:1 CCN47 + CB15) and with the same cell gap (12 μm). One has an aligned coating of elvamide polymer (continuous lines), whereas the other one has untreated glass substrates (dashed lines). The color code is the same as in the main text, with black lines representing the spectra through crossed polarizers, and the green and red lines being the spectra with the analyzer decrossed with an angle of respectively $+10°$ and $-10°$.

Because the ratio d/p gives the number of pitches across the cell, we can estimate the width of the pitch distribution as $\Delta p \sim p^2/d$, and we incorporated it into the calculation. Its effect is to partly broaden and smooth the spectra, as shown in Fig. 2*A* (main text) of the main article, where we have plotted, for comparison, a spectral dependence computed with no correction for strain (dotted red line).

1.7 Ionic strength dependence of the N^* pitch. To test the dependence of the N^* pitch from ionic strength, we studied the phase behavior of DD, for a concentration near the I-N^* boundary, whereas adding different amounts of the monovalent ion Na^+. Namely, we measured pitch sign and absolute value for various concentrations of added NaCl or NaOH, 0.5 M to 2 M. The results are shown in the Fig. S3: no systematic variation was observed in the pitch, as reported in (4) for longer DNA [although a more recent investigation finds a pitch drop around 30% between 0.2 and 1 M NaCl (5)].

This basic independence of N^* pitch from added ions is likely related to the high concentration required to observe the N^* phase in nDNA: $c_{IN} \approx 750$ mg/ml for DD, this value itself only weakly depending on ionic strength. Such high DNA concentration makes the effective counterion concentration always larger than 2 M (6) (and thus $\lambda_D < 0.5$ nm) and weakens the effect of added ions.

This finding agrees with what previously reported for longer DNA (4), but contrasts with recent results describing a drop in the pitch value between 0.2 and 1 M NaCl (4).

1.8 Previous observation of short pitch in DNA LC. Short pitches, with reflections in the in the visible range, appear to be a distinctive attribute of short nDNA. In the ample literature on long DNA LCs, 150 to thousands bp, average values of 2 to 4 μm are reported (and predicted by the current models). To our knowledge, there is a single report of submicrometric pitch for 150 bp DNA (and longer, sonicated DNA) (7), presented as a rare phenomenon and only obtained in presence of K^+ or multivalent ions in progressively dehydrated samples. In nDNA samples, instead, the occurrence of submicrometric pitch is a recurrent property of specific sequences and is completely absent in the others, despite the wide range of experimental conditions explored, including the dehydration process.

1.9 Pitch prediction from Straley's model of interacting chiral rods. The basic expectation for the dependence of pitch on effective oligomer length L can be obtained from Straley's model of interacting chiral hard rods (8), which yields an evaluation of K_{22} and K_t for a system of rods of length L, diameter D and number density N_d. The model predicts $K_{22} \sim N_d^2 L^4 D k_B T$ and $K_t \sim N_d^2 L^2 S^2 \Delta D k_B T$, where S is the nematic order parameter and Δ is the length characterizing the chiral steric protrusions on the rods. Note that K_{22} in not predicted to depend on the order parameter. On the basis of $p = 2\pi K_{22}/K_t$, we obtain:

$$p \propto \frac{L^2}{S^2 \Delta}. \qquad \textbf{[S5]}$$

Because all the explicit dependencies from temperature and concentration cancel out, for a given system S remains as the only parameter affecting the pitch. Eq. **S5** enables to compare nematics made of rods of different length. Simulations indicate that the nematic order parameter at the isotropic-nematic (IN) transition (i.e. found when moving along the Onsager line in the c—L/D plane) depends rather weakly, less than linearly, on L (9). If we assume that this is true also in the present case where the Onsager criterion is met by linear aggregates of oligomers, we obtain from Eq. **S5** that p is in general expected to be shorter in systems of shorter rods. This would appear to be a basic explanation for the appearance of shorter pitches in shorter DNAs.

Straley's model, based on pure steric interactions, acquire more significance in nDNA because of the larger concentration at which the phases are found.

1.10 Additional discussion on the concentration dependence of the N^* pitch. A reference case in understanding the concentration dependence of the N^* pitch is provided by the behavior of 150 bp DNA. Its N^* phase is in the concentration range 150–380 mg/mL, as estimated by Livolant et al. (10). The LH pitch is in the 2–4 μm range and depends nonmonotonically on c, with the shortest pitch in the middle of the N^* phase. Pitch increases as the I-N^* transition concentration is approached because of the reduced nematic order within the phase (as reflected in the dependence $p \propto S^{-2}$ in Eq. **S5**), and it increases approaching the concentration of the N^*-COL transition because fluctuations of local columnar order tend to expel the twist, and parallel packing prevails over chiral torque. Should the tendency for columnar order be suppressed, the trend of the pitch would be to continue decreasing with increasing concentration. The shift of both the N^* and the columnar range to larger concentration could account for the fact that LH nDNA, exploring more highly packed N^* than long DNA, features shorter pitches, whereas the dependence of $|p|$ on c for each sequence is dominated by the approach to the columnar phase (always observed in the phase diagrams) and is thus that of a monotonic increase.

Data suggest that, as the concentration is further increased, a new regime sets in. For some mechanism, the interhelical coupling is inverted and the favored symmetry is RH, in some cases dominating over the effect of approaching the N^*-COL boundary. This appears to be what happens to allCG2 and DD-RNA (11), where the N^* phase is free to wind up with RH symmetry.

Pitch inversion as a function of distance or concentration has not been explicitly predicted by either the Tombolato–Ferrarini (TF) or the Kornyshev–Leikin (KL) models. In both, however, the calculated behavior is the result of competing terms, a condition that has the potential for a rich phenomenology. Specifically, in TF model, the competing factors are the steric and electrostatic interactions, that give rise to torques typically having opposite signs (12). In KL model, instead, where steric interac-

tions are not included, conflicting trends come from the different "helical harmonics" of the potential generated by the double helical pattern of charges. The two lowest terms in the expansion favor two different azimuthal orientations of the helices, which in turn could favor opposite twists (13). Hence, it appears conceivable that both models, if explored in a wider range of parameters, could account for our observations.

1.11 Temperature dependence of the N^* pitch. The dependence of the pitch of the N^* phase of nucleic acids on temperature (T) is complex. While the N^* helix unwinds as T is increased in DNA solutions, it behaves oppositely in the case of G-wires. It has been noted that the extrapolation at large T would yield a pitch reversal for the DNA N^* phase, and it was suggested that the DNA and G-quartet behavior may be both resulting from a competitive balance between enthalpic (mainly electrostatic) interactions favoring a LH supramolecular arrangement and entropic (steric) interactions favoring instead a RH structure (14). In this view, the DNA behavior is dominated by electrostatic interactions, whereas for the G-wires handedness is driven by steric interactions. Conflicting interactions—in conjunction with the dynamic equilibrium between isomers of opposite chirality—have also been invoked to account for the handedness reversal described for various systems in the broader context of the N^* phase of thermotropics and polymer solutions (15—17). On the theoretical side, explicit calculations of $p(T)$ have been performed for DNA in the frame of TF model, leading to predictions in line with the observed DNA behavior.

For most of the sequences, as T is raised the N^* helix unwinds, as reported in Table 1, regardless of the handedness of the phase. In the Fig. S4, we show this behavior through PTOM pictures taken at different T in a LH short pitch compound (allAT, A and B) and in a RH long pitch sample (DD, C and D). In the latter case, as T increases, the N^* helix, detectable through the fingerprint patterns, completely unwinds forming a nonchiral nematic phase (panel 5d). This behavior is however not universal, because four exceptions have been found among the investigated sequences: in one of the 8-mers (8sc2, LH), in pDD and DDp (RH), and in the high concentration, RH branch of allCG2, shown in E and F, where shrinkage of p vs. T is visible [in (F), p approaches the optical resolution limit]. Picture sides are 100 μm (A and B) and 50 μm (C–F).

A quantitative analysis of the T dependence of p is shown in Fig. S5. Specifically, in the figure we display $q = 2\pi/p$ vs. $1/T$ for the N^* phase of 9 different compounds, the largest T in each set being ~2 °C below the melting T. The sign of q reflects the N^* handedness.

1.12 Discussion of the temperature dependence of the N^* pitch. As shown in Fig. S5, most of the investigated nDNA sequences, $|p|$ grows with T. The same trend is found in the N^* phase of long DNA, whereas G-quartets behave oppositely (14). To unify the T dependence observed in long DNA, in G-quartets from nucleotide guanosine-monophosphate and in poly guanosine, ref. 14 proposes a simple model, based on assuming the helix interactions as due to the conflicting combination of steric exclusion among rigid, T-independent B-DNA structures and of electrostatic interaction between the charged helical phosphate chains. In this frame, as T grows the soft electrostatic interactions become less effective, and $|p|$ is increasingly determined by the steric part. Such picture could appear to explain at least qualitatively the behavior of allCG2 reported in the figure. At lower concentrations and low T the electrostatic coupling prevails, a situation that enables us to identify as LH the symmetry of such interaction. At T grows, the electrostatic term fades and $|p|$ decreases to approach the RH symmetry favored by the steric locking. At larger c, the same picture is true, but the steric interactions are more relevant so to dominate in the resulting handedness.

The whole set of results in the figure and in Table 1 (main article), however, indicates that this description is inadequate for most of the other sequences showing pitch unwinding. The decrease of the chiral strength with T would imply that for both signs of handedness, the chirality is promoted by electrostatic interactions. Namely, the RH N^* of, for example, DD would be promoted by electrostatic interactions winning over LH steric interaction, whereas the exact opposite would be true for the LH N^* phase of, for example, GC-DD. This appears as a rather unreasonable assumption, given the minor structural and electrical difference between compounds yielding LH vs. RH phases. An equally striking contradiction would hold while comparing DD and pDD behavior. Furthermore, the fact that no sequences have been found where the sign of p inverts with T, indicates that the interpretation of ref. 14 cannot be applied here.

Indeed, interpreting the behavior of $|p|$ that grows or decreases with T depending on the sequence (both for RH and LH cholesterics), is a challenge. The fact that the nematic ordering of nDNA is promoted by the linear aggregation of the duplexes, in turn T-dependent, makes any prediction quite complex. As T increases, the length ℓ of the duplex aggregate decreases while its flexibility increases, until the combination (c, ℓ) drops below the Onsager line. As a consequence, analogously to thermotropics (3) but differently from typical lyotropic N^* phases, the quantities K_t and K_{22} both decrease as T increases approaching T_{IN}. The progressive disruption of the N^* ordering with T is testified by the T dependence of the birefringence Δn, dropping of 30–50% as the phase melting is approached, indicating substantial loss of order. According to $p = 2\pi K_{22}/K_t$, $p(T)$ depends from the relative strength of the T dependence of K_t and K_{22}. Whereas $K_{22}(T)$ could be somehow estimated from $\Delta n(T)$ (and may depend on the aggregate length), for $K_t(T)$ we definitely lack information, especially given the many ingredients it could depend on. The variety of the observed behavior suggests that the functional form of $K_t(T)$ is a variable function of T. Given the complexity of the interactions at play in the TF and KL model, this could indeed be a realistic possibility. Indeed, a recent model adds to the hard core and to the chiral electrostatic potentials an achiral attractive or repulsive soft potential (18). Within this frame, the N^* pitch can display nonmonotonic T-dependence, and the position of its minimum is tuned by the strength of the achiral interaction. For instance, this may suggest an explanation for the different behavior of DD and pDD or DDp, only differing in the presence of additional charged groups.

1.13 Other factors affecting handedness and periodicity of the N^* phase. Flexibility. Another helical property that in principle could affect the N^* handedness is the flexibility of the helices. It is known that different patterning in flexibility play a role in the propagation of chirality, as found for the nematic ordering of assemblies of filamentous viruses whose capsid proteins are helically arranged with RH parity. It has been observed that subtle changes in the capsid flexibility have huge effects on the N^* pitch, including handedness inversion (19) and loss of phase chirality (20). This phenomenon has been interpreted as mediated by superhelical twisting of the capsid. The N^* properties of nDNA, however, show no evidence supporting a role of flexibility. The tabled elastic properties of nucleotides indicate that CG steps are typically more flexible than AT steps (21, 22), whereas the sequences allAT and allCG1—supposedly differing in flexibility—have the same handedness.

Structure of the linear aggregates. Among the structures reported for nDNA duplexes in hydrated crystals an interesting example of curved arrangement is the coiled coil found for the sequences ATATATATATAT and CGATATATATAT (23). These sequences form linear aggregates via SD linking. Although these are sequences that we haven't explored because their pairing and/or

SD aggregation is not unique, this behavior further confirms the possibility of bent structures in aggregated oligomer duplexes.

2 SI Materials and Methods. Synthetic oligonucleotide sequences listed in Table 1, purified by HPLC, were purchased from Primm as liophylized powders. Concentrated solutions (200–1000 mg/mL) were prepared by dissolving them in MilliQ-filtered water. In specific cases, solutions were prepared with added NaCl or NaOH to test for dependence on ionic strength. The solutions were loaded between parallel plate glass plates separated by thin polyethylene terephthalate film stripes or silica rods, obtaining gap d in the range 5–30 μm. In some cells, evaporation was exploited to produce concentration gradients, a condition enabling observation of the corresponding gradient in the N^* pitch. In the cells aimed at quantitative analysis, the solution drop was sealed with a fluorinated oil and generally left for at least 1 hour at 60 °C to let the DNA concentration homogenize. In reference cells with thermotropic LCs (CCN47 and CB15 from Merck, cholesteryl esthers from Varilight Corporation), glass surfaces were treated, when needed, with an elvamide polymer solution, spin-coated on the surface and rubbed to promote planar alignment in a specific direction. Microscopic observations were made either on a Nikon TE200 or on a Nikon Optiphot2 microscope. Images were acquired on a Nikon DS-5M camera.

To measure the handedness of the N^* phase, spectra were acquired with a S200 UV-VIS spectrometer (Ocean Optics) connected to the TE200 microscope. The analyzer position was scanned while keeping sample and polarizer positions fixed, and spectra were averaged over different positions of the polarizer. The obtained curves were fitted with the model discussed above.

To measure solution concentration, cells made with high-refractive index glass (F2 Schott, $n = 1.62$) were brought, through heating, into the isotropic phase where the spectrum of the reflected intensity was measured. The frequency of the multiple reflection fringes due to the interference from the parallel cell plates, was systematically measured in various spots within the DNA solution and on the periphery of the cells, where the fluorinated oil was instead present. This set of data enabled determining the refractive index of the DNA solution and thus the DNA concentration c through a calibration curve. These values have an uncertainty of about ±50 mg/mL. Surface and interaxial separations were calculated from the concentration values assuming local hexagonal packing, helix radius $R = 1.0$ nm and density 1.8 g/cm^3. The temperature dependence of the pitch was measured either through the shift of the peak in the reflectance spectrum, or from the change in the extinction angle.

1. Wing R, et al. (1980) Crystal structure analysis of a complete turn of B-DNA. *Nature* 287:755–758.
2. Yang D, Mi X (2000) Modelling of the reflection of cholesteric liquid crystals using the Jones matrix. *J Phys D Appl Phys* 33:672–676.
3. Chandrasekhar S (1992) *Liquid Crystals* 2nd Ed (Cambridge University Press, Cambridge, UK).
4. Van Winkle DH, Davidson MW, Chen WX, Rill RL (1990) Cholesteric helical pitch of near persistence length DNA. *Macromolecules* 23:4140–4148.
5. Stanley CB, Hong H, Strey HH (2005) DNA cholesteric pitch as a function of density and ionic strength. *Biophys J* 89:2552–2557.
6. Nakata M, et al. (2007) End-to-end stacking and liquid crystal condensation of 6- to 20-base pair DNA duplexes. *Science* 318:1276–1279.
7. Leforestier A, Livolant F (1993) Supramolecular ordering of DNA in the cholesteric liquid crystalline phase: An ultrastructural study. *Biophys J* 65:56–72.
8. Straley JP (1976) Theory of piezoelectricity in nematic liquid crystals, and of the cholesteric ordering. *Phys Rev A* 14:1835–1841.
9. Bolhuis P, Frenkel D (1997) Tracing the phase boundaries of hard spherocylinders. *J Chem Phys* 106:666–687.
10. Livolant F, Leforestier A (1996) Condensed phases of DNA: Structures and phase transitions.*Prog Polym Sci* 21:1115–1164.
11. Zanchetta G, Nakata M, Bellini T, Clark NA (2008) Physical polymerization and liquid crystallization of RNA oligomers. *J Am Chem Soc* 130:12864–12865.
12. Tombolato F, Ferrarini A (2005) From the double-stranded helix to the chiral nematic phase of B-DNA: A molecular model. *J Chem Phys* 122:054908.
13. Kornyshev AA, Lee DJ, Leikin S, Wynvenn A (2007) Structure and interactions of biological helices. *Rev Mod Phys* 79:943–996.
14. Proni G, Gottarelli G, Mariani P, Spada GP (2000) The chirality of the cholesteric phases of DNA and G-wires: Its connection to their molecular structures. *Chem Eur J* 6:3249–3253.
15. Watanabe J, Nagase T (1988) Thermotropic polypeptides. 5. Temperature dependence of cholesteric pitches exhibiting a cholesteric sense inversion. *Macromolecules* 21:171–175.
16. Watson MJ, et al. (1998) A phenomenological approach to the inversion of the helical twist sense in the chiral nematic phase. *J Mater Chem* 8:1963–1969.
17. Sato T, et al. (1993) Polyisocyanates and the interplay of experiment and theory in the formation of lyotropic cholesteric states. *Macromolecules* 26:4551–4559.
18. Wensink HH, Jackson G (2009) Generalized van der Waals theory for the twist elastic modulus and helical pitch of cholesterics. *J Chem Phys* 130:234911.
19. Barry E, Beller D, Dogic Z (2009) A model liquid crystalline system based on rodlike viruses with variable chirality and persistence length. *Soft Matter* 5:2563–2570.
20. Tomar S, Green MM, Day LA (2007) DNA–protein interactions as the source of large-length-scale chirality evident in the liquid crystal behavior of filamentous bacteriophages. *J Am Chem Soc* 129:3367–3375.
21. Packer MJ, Dauncey MP, Hunter CA (2000) Sequence-dependent DNA structure: Dinucleotide conformational maps. *J Mol Biol* 295:71–83.
22. Fujii S, Kono H, Takenaka S, Go N, Sarai A (2007) Sequence-dependent DNA deformability studied using molecular dynamics simulations. *Nucleic Acids Res* 35:6063–6074.
23. De Luchi D, Tereshko V, Gouyette C, Subirana JA (2006) Structure of the DNA coiled coil formed by d(CGATATATATAT).*Chem Bio Chem* 7:585–587.

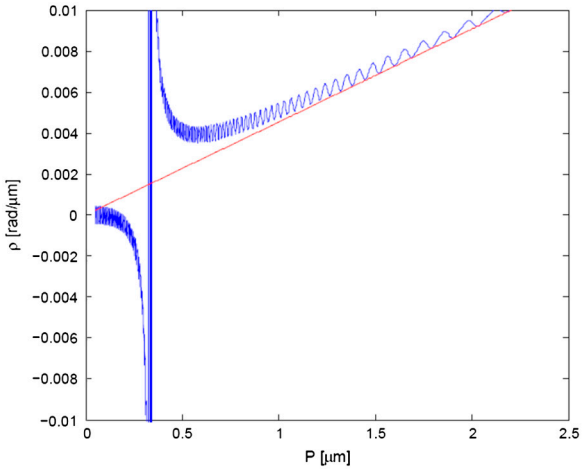

Fig. S1. Comparison between the optical rotation computed by with Eq. **S2** (red line) and obtained through the propagation model described above (blue line). Tin both cases $n = 1.5$, $\Delta n = 0.038$, $h = 15$ μm, $\lambda = 0.5$ μm.

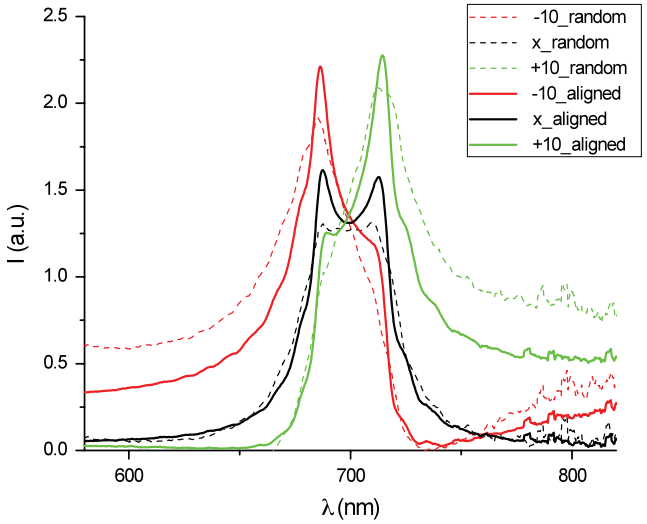

Fig. S2. Transmission spectra for two different cells containing the same thermotropic mixture M2 (2:1 CCN47 + CB15) and with the same cell thickness (12 μm). Continuous lines: homogeneous planar anchoring. Dashed lines: random planar anchoring (untreated glass). Black lines: *r* crossed polarizers. Green and red lines: spectra with the analyzer decrossed with angles of +10° and −10° respectively.

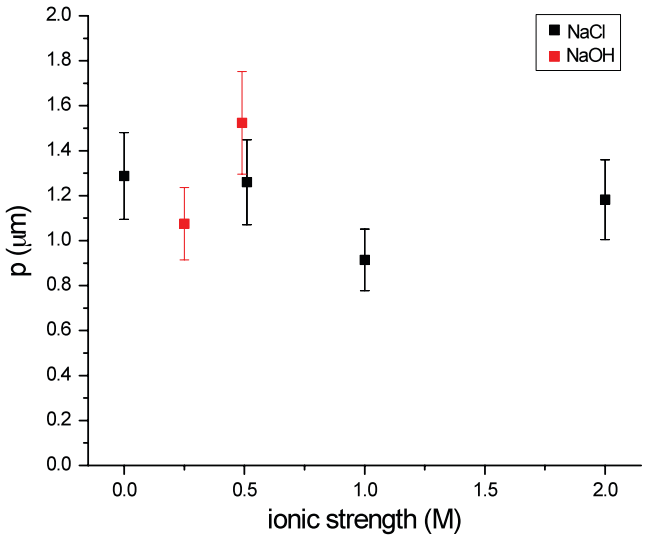

Fig. S3. N^* pitch as a function of the ionic strength measured for DD at a concentration near the *I*-N^* boundary. Monovalent Na^+ counterions are introduced by adding NaCl (black symbols) or NaOH (red symbols) to the solution.

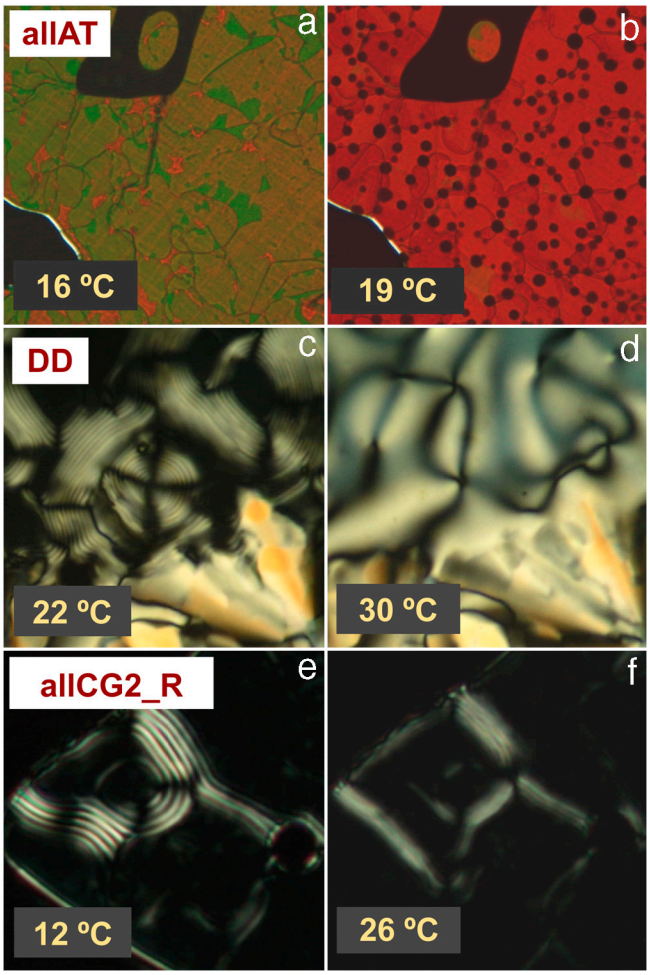

Fig. S4. Temperature dependence of the N^* pitch in nDNA samples. (*A*, *B*) Increase of *p* vs. *T*, revealed by the selective transmission through cross polarizers, in allAT. (*C*, *D*) Divergence of *p* in a DD sample while approaching the IN transition. (*E*, *F*) Shrinkage of *p* vs. *T* in the RH N^* branch of allCG2 [in (*F*), *p* approaches the optical resolution limit]. Picture sides are 100 μm (*A*, *B*) and 50 μm (*C*–*F*).

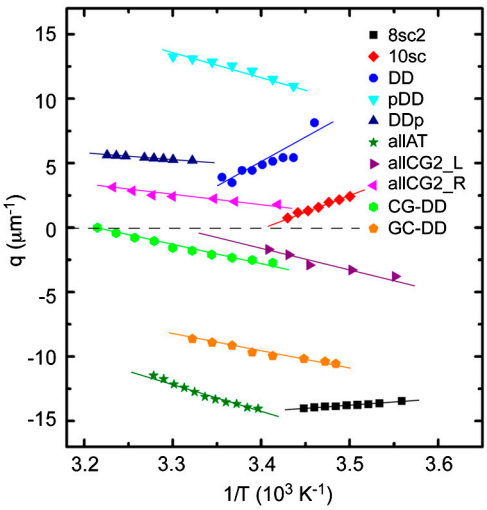

Fig. S5. Temperature dependence of the N^* inverse pitch in nDNA samples.